Assessing the relationship between microwave vegetation optical depth and gross primary production

Irene E. Teubner[a,*], Matthias Forkel[a], Martin Jung[b], Yi Y. Liu[c], Diego G. Miralles[d], Robert Parinussa[e], Robin van der Schalie[e], Mariette Vreugdenhil[a], Christopher R. Schwalm[f,g], Gianluca Tramontana[h], Gustau Camps-Valls[i], Wouter A. Dorigo[a]

[a] *Department of Geodesy and Geoinformation, TU Wien, Gußhausstraße 27-29, 1040 Vienna, Austria*
[b] *Department for Biogeochemical Integration, Max Planck Institute for Biogeochemistry, P.O. Box 10 01 64, 07701 Jena, Germany*
[c] *School of Geography and Remote Sensing, Nanjing University of Information Science & Technology (NUIST), No.219, Ningliu Road, Nanjing, Jiangsu, 210044, China*
[d] *Laboratory of Hydrology and Water Management, Ghent University, Campus Coupure, Coupure links 653, B-9000 Ghent, Belgium*
[e] *VanderSat B.V., Huygensstraat 34, 2201 DK Noordwijk, The Netherlands*
[f] *Woods Hole Research Center, 149 Woods Hole Road, Falmouth, MA, 02540-1644, USA*
[g] *Center for Ecosystem Science and Society, Northern Arizona University, P.O. Box 5620, Flagstaff, AZ 86011, USA*
[h] *Department for Innovation in Biological Agro-food and Forest systems (DIBAF), Tuscia University, Via San Camillo de Lellis s.n.c.- 01100 Viterbo, Italy*
[i] *Image and Signal Processing Group (ISP), Universitat de València, Calle Catedrático José Beltrán 2, 46980 Paterna (València), Spain*

Abstract

At the global scale, the uptake of atmospheric carbon dioxide by terrestrial

*Corresponding author

Email addresses: irene.teubner@geo.tuwien.ac.at (Irene E. Teubner), matthias.forkel@geo.tuwien.ac.at (Matthias Forkel), mjung@bgc-jena.mpg.de (Martin Jung), yiliu001@gmail.com (Yi Y. Liu), diego.miralles@UGent.be (Diego G. Miralles), rparinussa@vandersat.com (Robert Parinussa), rvanderschalie@vandersat.com (Robin van der Schalie), Mariette.Vreugdenhil@geo.tuwien.ac.at (Mariette Vreugdenhil), cschwalm@whrc.org (Christopher R. Schwalm), g.tramontana@unitus.it (Gianluca Tramontana), gcamps@uv.es (Gustau Camps-Valls), Wouter.Dorigo@geo.tuwien.ac.at (Wouter A. Dorigo)

Preprint submitted to International Journal of Applied Earth Observation and Geoinformation October 13, 2017

ecosystems through photosynthesis is commonly estimated through vegetation indices or biophysical properties derived from optical remote sensing data. Microwave observations of vegetated areas are sensitive to different components of the vegetation layer than observations in the optical domain and may therefore provide complementary information on the vegetation state, which may be used in the estimation of Gross Primary Production (GPP). However, the relation between GPP and Vegetation Optical Depth (VOD), a biophysical quantity derived from microwave observations, is not yet known. This study aims to explore the relationship between VOD and GPP. VOD data were taken from different frequencies (L-, C-, and X-band) and from both active and passive microwave sensors, including the Advanced Scatterometer (ASCAT), the Soil Moisture Ocean Salinity (SMOS) mission, the Advanced Microwave Scanning Radiometer for Earth Observation System (AMSR-E) and a merged VOD data set from various passive microwave sensors. VOD data were compared against FLUXCOM GPP and Solar-Induced chlorophyll Fluorescence (SIF) from the Global Ozone Monitoring Experiment-2 (GOME-2). FLUXCOM GPP estimates are based on the upscaling of flux tower GPP observations using optical satellite data, while SIF observations present a measure of photosynthetic activity and are often used as a proxy for GPP. For relating VOD to GPP, three variables were analyzed: original VOD time series, temporal changes in VOD (ΔVOD), and positive changes in VOD ($\Delta VOD_{\geq 0}$). Results show widespread positive correlations between VOD and GPP with some negative correlations mainly occurring in

dry and wet regions for active and passive VOD, respectively. Correlations between VOD and GPP were similar or higher than between VOD and SIF. When comparing the three variables for relating VOD to GPP, correlations with GPP were higher for the original VOD time series than for ΔVOD or $\Delta\text{VOD}_{\geq 0}$ in case of sparsely to moderately vegetated areas and evergreen forests, while the opposite was true for deciduous forests. Results suggest that original VOD time series should be used jointly with changes in VOD for the estimation of GPP across biomes, which may further benefit from combining active and passive VOD data.

Keywords: microwave remote sensing, vegetation dynamics, ecosystem productivity, ASCAT, SMOS, AMSR-E

---

1. Introduction

Vegetation plays an important role in the Earth system as plants take up atmospheric carbon dioxide through photosynthesis and transport water from the soil into the atmosphere through transpiration (Lambers et al., 2008). In addition, vegetation can influence the Earth's surface energy balance through differences in surface albedo compared to bare soil or snow cover, which is especially pronounced for boreal forests (Bonan, 2008). Therefore, monitoring the vegetation state in terms of photosynthetic activity as well as plant water status is of importance for hydrological, ecological and climate change applications (Bonan, 2015).

The uptake of atmospheric carbon dioxide by vegetation through pho-

tosynthesis is commonly referred to as Gross Primary Production (GPP) and is the largest carbon flux in the global carbon cycle (Ciais et al., 2013). GPP can be determined at site level from eddy covariance measurements of carbon dioxide net exchange, which is partitioned into GPP and ecosystem respiration (Baldocchi et al., 2001; Reichstein et al., 2005; Jung et al., 2011; Lasslop et al., 2012). Another approach is the biometric method, which combines estimates of plant growth, chamber flux measurements and stock inventories (Campioli et al., 2016). GPP can be assessed from local to global scales using process-based models that describe the canopy light absorption and the energy and enzyme limitations of the carboxylation rate to estimate gross carbon assimilation (e.g. Farquhar et al., 1980; Collatz et al., 1992). However, current process-based models show large uncertainties because of a limited understanding of the processes that are involved in photosynthesis (Rogers et al., 2017). Alternatively, data-driven approaches that combine satellite observations with empirical models can be used to estimate GPP at large scales (Beer et al., 2010).

Most of the approaches to estimate GPP from satellite observations use optical data to characterize biophysical properties or photosynthetic activity. Biophysical properties such as the Fraction of Absorbed Photosynthetically Active Radiation (FAPAR) are used in light-use efficiency models to estimate GPP, assuming a linear relationship between FAPAR and GPP which is modulated by temperature and water stress (Monteith, 1972; Nemani et al., 2003). Additionally, machine learning algorithms, driven by meteorological

and/or satellite data, have been used to upscale site-level observations of GPP (Beer et al., 2010; Jung et al., 2011; Tramontana et al., 2016). Alternatively, Solar-Induced chlorophyll Fluorescence (SIF), an estimate of photosynthetic activity, has been proposed as a global proxy for GPP in recent years (Frankenberg et al., 2014; Guanter et al., 2014; Damm et al., 2015; Zhang et al., 2016).

Optical remote sensing data, however, are often affected by clouds and aerosols (Myneni et al., 2002; Forkel et al., 2013) and sun-sensor geometry (Dorigo, 2012; Morton et al., 2014). A common method to reduce the influence of cloud cover on optical data is temporal compositing (Huete et al., 2011; Holben, 1986), which decreases the native temporal resolution. Alternatively, time series filtering can be applied (Chen et al., 2004).

In contrast to optical data, microwave radiation below a frequency of 10 GHz is less influenced by clouds and is independent of the sun as source of illumination (Woodhouse, 2005). Microwave satellite observations over vegetation are thus able to provide crucial information in areas with extensive cloud cover like the tropics or high latitudes. The penetration depth of the microwave radiation into the vegetation canopy depends on frequency, dielectric properties, size and geometry of the interacting vegetation parts. As such, microwave observations from different frequencies theoretically contain information from different parts of the vegetation (Woodhouse, 2005). Whereas high frequencies (short wavelengths) predominantly interact with small structures like leaves and twigs at the top of the vegetation layer, low

frequencies (long wavelengths) can penetrate deeper into the vegetation and are more sensitive to large structures like branches or trunks (Woodhouse, 2005). Accordingly, microwave radiation exhibits a higher penetration depth than optical radiation due to its longer wavelength, and should theoretically be better suited for monitoring denser canopies, as the observed signal does not saturate as quickly as for optical sensors (Woodhouse, 2005; Dorigo et al., 2007). Therefore, microwave satellite observations have the potential to provide valuable information on the vegetation state complementary to optical satellite data which are traditionally used for estimating GPP.

Microwave Vegetation Optical Depth (VOD) describes the attenuation of radiation due to scattering and absorption within the vegetation layer, which is caused by the water contained in the vegetation (Woodhouse, 2005). At low biomass, VOD is linearly related to the vegetation water content (VWC; expressed in kg/m^2) (Jackson and Schmugge, 1991; Woodhouse, 2005). In addition, VOD can be related to aboveground living biomass (Liu et al., 2015; Tian et al., 2016) and to Leaf Area Index (LAI), especially in crop- and grasslands (Zribi et al., 2011; Kim et al., 2012; Sawada et al., 2016).

VOD data have been analyzed for different applications such as long-term trends in biomass (Andela et al., 2013; Liu et al., 2013a,b, 2015), forest loss (Marle et al., 2016), phenology metrics (Jones et al., 2011, 2012), vegetation water stress (Miralles et al., 2016), evaporation retrievals (Miralles et al., 2011; Martens et al., 2016) and ecosystem resilience (Verbesselt et al., 2016). However, short-term variations in VOD have not been assessed with regard

to GPP.

The aim of this study is to explore the relationship between VOD and GPP and assess if VOD can provide additional information about GPP on top of what is provided by SIF. In addition, this study investigates the effect of different microwave frequencies (between 1 and 10 GHz) and of active and passive sensors (hereafter referred to as active and passive VOD) on the relationship between VOD and GPP.

2. Data and methods

2.1. Vegetation remote sensing data

The analysis is based on five VOD data sets, upscaled GPP estimates, and SIF observations (Table 1). The data sets have different temporal coverage with a common overlap of about one year. The period from January 2007 to December 2015 was selected in order to obtain a minimum number of four years of overlap with the GPP data set.

2.1.1. VOD ASCAT

Active microwave VOD data were retrieved from microwave backscatter measurements of the Advanced Scatterometer (ASCAT) onboard the meteorological operational satellite A (MetOp-A). ASCAT measures backscatter at 5.25 GHz (C-band) in vertical co-polarization. The retrieval of VOD is based on slope estimates of the angular backscatter dependency, which are calculated during the soil moisture retrieval using the TU-Wien change detection

algorithm. VOD is obtained by relating the angular sensitivity of measured backscatter to the sensitivity of modelled bare soil backscatter (Melzer, 2013; Vreugdenhil et al., 2016a,b) and, therefore, represents a measure of volume scattering due to vegetation relative to bare soil volume scattering. VOD is derived jointly from measurements in ascending and descending mode (9:30 a.m./p.m. equatorial crossing).

2.1.2. VOD AMSR-E

Measurements at 6.9 GHz (C-band) and 10.7 GHz (X-band) were used from the Advanced Microwave Scanning Radiometer for Earth Observation System (AMSR-E). For both frequencies, VOD was obtained with the Land Parameter Retrieval Model (LPRM) v06 (van der Schalie et al., 2017). The algorithm uses a radiative transfer model (Mo et al., 1982) and includes an analytical solution for VOD using the Microwave Polarization Difference Index (MPDI) (Meesters et al., 2005). LPRM retrieves VOD and soil moisture simultaneously under the assumption of a globally constant single scattering albedo and further assumes that soil and canopy temperature are similar (Owe et al., 2001). Since the latter assumption generally does not hold for daytime observations, we only used observations from the descending mode for this analysis (1:30 a.m. equatorial crossing).

2.1.3. VOD SMOS

VOD from the Soil Moisture Ocean Salinity (SMOS) radiometer, which provides observations at 1.4 GHz (L-band), was also retrieved with the LPRM

v06 (van der Schalie et al., 2016, 2017). Only data from the ascending mode were analyzed (6 a.m. equatorial crossing) as soil and canopy temperatures are usually more similar in the morning than in the late afternoon although seasonal and latitudinal variations exist.

2.1.4. VOD merged

In addition to the single frequency data sets, a merged passive microwave VOD data set developed by Liu et al. (2015) was included in this analysis. For the period 2007-2012, the data set comprises observations from AMSR-E (6.9 GHz, C-band), WindSat (6.8 GHz, C-band), and the FengYun-3B Microwave Radiometer Imager (10.7 GHz, X-band). Prior to merging, the single sensor data sets were rescaled by applying the cumulative distribution function (CDF) matching technique with AMSR-E as the reference (Liu et al., 2009).

2.1.5. GPP FLUXCOM

The FLUXCOM GPP data set presents an upscaling of flux tower measurements based on multiple machine learning algorithms and satellite data (Tramontana et al., 2016). Different remotely sensed data in the optical domain from the Moderate Resolution Imaging Spectroradiometer (MODIS) were used as input, including the Enhanced Vegetation Index (EVI), LAI, band 7 - Middle Infrared Reflectance (MIR), Normalized Difference Vegetation Index (NDVI), and Normalized Difference Water Index (NDWI) (Tramontana et al., 2016).

Table 1: Data set overview. Acronyms: Enhanced Vegetation Index (EVI), Leaf Area Index (LAI), MODIS band 7 - Middle Infrared Reflectance (MIR), Normalized Difference Vegetation Index (NDVI), Normalized Difference Water Index (NDWI), and Land Parameter Retrieval Model (LPRM).

Name	Data set	Period used	Frequency/ wavelength/ data input	Spatial resolution	Temporal resolution	Type	Method/ algorithm	Reference
SMOS	SMOS	7/2010 - 12/2015	1.4 GHz	0.25°	Daily	Passive microwave	LPRMv06	van der Schalie et al. (2017)
ASCAT	ASCAT	1/2007 - 12/2015	5.25 GHz	12.5 km	Daily	Active microwave	TU-Wien change detection	Melzer (2013); Vreugdenhil et al. (2016a,b)
AMSRE_C	AMSR-E	1/2007 - 9/2011	6.9 GHz	0.25°	Daily	Passive microwave	LPRMv06	van der Schalie et al. (2017)
AMSRE_X	AMSR-E	1/2007 - 9/2011	10.7 GHz	0.25°	Daily	Passive microwave	LPRMv06	van der Schalie et al. (2017)
VODmerged	AMSR-E, WindSat, FY-3B	1/2007 - 9/2011, 1/2007 - 6/2012, 11/2010 - 12/2012	6.9 GHz, 6.8 GHz, 10.7 GHz	0.25°	Daily	Passive microwave	LPRMv05	Liu et al. (2015)
GPP	FLUXCOM	1/2007 - 12/2015	MODIS EVI, LAI, MIR, NDVI, NDWI	10 km	8-daily	Optical	Machine learning	Tramontana et al. (2016)
SIF	GOME2_F v26	1/2007 - 12/2015	740 nm	0.5°	Monthly	Optical		Joiner et al. (2013, 2014)

2.1.6. SIF GOME-2

The GOME-F v26 SIF data were obtained from the Global Ozone Monitoring Experiment-2 (GOME-2) sensor. The retrieval is based on the filling-in of Frauenhofer lines, which is caused by the chlorophyll fluorescence emitted from the Earth's surface (Joiner et al., 2013). The algorithm uses principal components analysis and radiative transfer theory to determine SIF at 740 nm (Joiner et al., 2013, 2014, 2016). In this study, SIF observations from the MetOp-A platform were used.

2.2. Ancillary data

2.2.1. CCI land cover

The European Space Agency (ESA) Climate Change Initiative (CCI) global land cover data set v1.6.1 was used for identifying homogenous grid cells and stratifying results according to land cover. The data set is derived from Medium Resolution Imaging Spectrometer (MERIS) surface reflectance time series and has a spatial resolution of 300 m (Bontemps et al., 2013). The maps are available for three epochs that cover the periods 1998-2002, 2003-2007, and 2008-2012, respectively. In this study, the map for the period 2008-2012 was used as it falls within the overall data period.

2.2.2. GPCP

Precipitation data from the Global Precipitation Climatology Project (GPCP) are displayed as reference in the time series plot. GPCP 1DD version 1.2 provides daily precipitation estimates at 1° spatial resolution (Huffman et al., 2001). The precipitation estimates are produced from satellite data in the high frequency microwave (>10 GHz) to infrared region in combination with gauge data (Huffman et al., 2001).

2.2.3. ERA-Interim

Skin temperature and snow depth from ERA-Interim were used to mask VOD. ERA-Interim is the current global atmospheric reanalysis produced by the European Centre for Medium-Range Weather Forecasts for the period from 1979 onwards (Dee et al., 2011). Data are assimilated using a

4-dimensional variational analysis. The horizontal resolution is about 0.7° at the equator.

2.2.4. Topographic complexity

Topographic complexity was used to mask VOD during the analysis of homogeneous grid cells. It is described by the standard deviation of elevation within a grid cell. A map of topographic complexity is available as ancillary data for the ESA-CCI soil moisture v02.2 data set (Dorigo et al., 2015) with a spatial resolution of 0.25°. The topographic complexity is computed from the USGS 30-Arc-Second Global Elevation Data Set (GTOPO30) (USGS, 1996).

2.3. Variables for relating VOD to GPP

In this study, three variables for comparing VOD with GPP are investigated: (1) original time series of VOD, (2) change in VOD (ΔVOD), and (3) positive changes in VOD ($\Delta \mathrm{VOD}_{\geq 0}$). The latter two variables treat VOD as a proxy for aboveground biomass of the vegetation layer, which includes leaves and woody components. Liu et al. (2015) showed that the relationship between VOD and forest biomass data is monotonically increasing, which makes VOD a suitable proxy for biomass. Changes in VOD may thus relate to changes in biomass and hence to Aboveground Net Primary Production (ANPP), which contributes to total Net Primary Production (NPP).

1) Original VOD time series: For crop- and grasslands, VOD is proportional to total VWC (Jackson and Schmugge, 1991; Woodhouse, 2005)

and thus scales with LAI (Zribi et al., 2011; Kim et al., 2012; Sawada et al., 2016), which in turn is related to GPP (Suyker et al., 2005; Gitelson et al., 2014). The original time series of VOD may thus be related to GPP.

2) ΔVOD: For forests, ANPP is commonly estimated through biomass changes between two consecutive measurements (Clark et al., 2001a; Campioli et al., 2011; Nunes et al., 2013; Wagner et al., 2013a; Campioli et al., 2016). Therein, biomass changes are determined from changes in stem circumference, which are converted to whole-tree biomass using allometric relations, and from litter traps or LAI. In this study, this method is adopted by calculating the change in VOD.

$$\Delta VOD(t) = VOD_t - VOD_{t-1}$$

where ΔVOD(t) is the change in VOD at time t, and VOD_t and VOD_{t-1} are VOD observations at time t and t-1, respectively.

3) $\Delta\text{VOD}_{\geq 0}$: For grasslands, common metrics for determining annual ANPP include peak standing biomass, difference between maximum and minimum standing biomass, sum of positive biomass changes with negative values set to zero, and change in biomass (Scurlock et al., 2002). These metrics are designed for a low number of observations as the sampling of herbaceous vegetation is destructive and is often carried out once per growing season. Since the study focuses on the temporal

agreement instead of annual metrics and the change in VOD is already analyzed as the second variable, the method of positive biomass changes is used as third variable.

$$\Delta VOD_{\geq 0}(t) = \begin{cases} \Delta VOD(t) & \text{if } \Delta\text{VOD(t)} \geq 0 \\ 0 & \text{otherwise} \end{cases}$$

In order to compare the results of all three variables, changes in VOD (ΔVOD and $\Delta\text{VOD}_{\geq 0}$) are also compared with the FLUXCOM GPP data set although, conceptually, they should relate more closely to NPP than GPP. However, direct measurements of large-scale NPP are not possible and, therefore, NPP is often derived from remote sensing-based GPP estimates using either a constant NPP:GPP ratio at annual time scales (Waring et al., 1998) or the difference between GPP and autotrophic respiration at shorter time scales (Running et al., 2004; Zhao et al., 2005). For this reason, VOD variables in this study are related to GPP and not to NPP.

2.4. Data preparation

The global data sets of VOD and GPP were resampled to a common resolution of 8 days and 0.25°. Resampling was performed by averaging over the 8-day period for VOD data sets or over the grid points within each 0.25° by 0.25° grid cell for GPP. Prior to the resampling of the daily VOD data sets, the data were masked for conditions of frozen soil or snow based on ERA-Interim. Observations were excluded if the daily mean skin temperature was

Table 2: CCI land cover abbreviations.

Abbreviation	CCI land cover class
CRO	Cropland, rainfed
EBF	Tree cover, broadleaved, evergreen, closed to open (>15%)
DBF	Tree cover, broadleaved, deciduous, closed to open (>15%)
ENF	Tree cover, needleleaved, evergreen, closed to open (>15%)
DNF	Tree cover, needleleaved, deciduous, closed to open (>15%)
SHR	Shrubland
GRA	Grassland
SPARSE	Sparse vegetation (tree, shrub, herbaceous cover) (<15%)

$\leq$0 °C or snow cover was present. For consistency with the VOD data sets, GPP and SIF were also masked accordingly. Passive microwave observations can be affected by radio frequency interference (RFI), which is caused by artificial sources of radiation and hence is not related to land surface properties (Li et al., 2004; Njoku et al., 2005). Therefore, passive VOD data were additionally masked for RFI. For ASCAT, negative values can occur due to a lower sensitivity of the modelled bare soil backscatter compared to the observed backscatter in the angular dependency (Vreugdenhil et al., 2016a). These negative values were not set to zero in order to avoid introducing a bias. For the comparison with SIF observations, GPP and VOD data sets were further resampled to monthly and 0.5° resolution using temporal and spatial means, respectively.

Land cover data were converted into fractional land cover at 0.25° (or 0.5°) resolution using the level 1 legend of the CCI classification scheme. The resulting map of dominant land cover at 0.25° resolution is displayed in Figure S1. The corresponding abbreviations are summarized in Tables 2 and S1. For global correlation maps, grid cells with a dominant land cover class of permanent snow/ice or water were systematically excluded.

For stratifying the results according to land cover, only homogeneous grid cells were evaluated in order to minimize the influence of pixel heterogeneity. Using the ESA CCI land cover map, a grid cell was considered homogeneous if the fraction of dominant land cover within a 0.25° by 0.25° grid cell exceeded an arbitrary threshold of 75%. Additionally, grid cells were discarded if either topographic complexity or percentage of water bodies were higher than 10% following Draper et al. (2012) and Dorigo et al. (2015), since both factors have a strong impact on the emitted or reflected microwave signal (Owe et al., 2008).

Data smoothing was applied in two cases: 1) prior to calculating changes in VOD (ΔVOD and $\Delta\text{VOD}_{\geq 0}$) and 2) for visualization purposes in the time series plots. The smoothing was performed using a Savitzky-Golay filter of order three with a window size of 11 observations.

2.5. Statistical analysis

Linear relationships were assessed using correlation analysis. Prior to the correlation analysis, the assumption of normality was tested following D'Agostino (1971) and D'Agostino and Pearson (1973). As not all grid cell data were normally distributed ($p>0.05$), the non-parametric Spearman rank correlation was used instead of the parametric Pearson correlation. Due to this absence of normal distribution for some grid cell data, non-parametric measures were used when analyzing full-length time series data: the median for displaying the global distribution of the data sets and the coefficient of

quartile variation (CQV, Kokoska and Zwillinger, 2000) for assessing signal variability. CQV is calculated using the 25th (Q1) and the 75th (Q3) percentile:

$$CQV = (Q3 - Q1)/(Q3 + Q1)$$

In addition to the zero-lagged correlation analysis, time lags for which the cross-correlations maximized were calculated as an additional measure to determine how well the signals match. Results for homogeneous grid cells are displayed as violin plots, which are similar to box plots but visualize the kernel estimation of the data distribution.

To compare the data sets independent of the strong seasonal signals that affect vegetation properties in many regions, anomalies relative to the mean seasonal cycle were calculated. The mean seasonal cycles were obtained from the 8-daily or monthly time series by averaging over each valid day in a year within the study period. Due to the relatively short data periods, no detrending was applied prior to calculating the mean seasonal cycles.

Residuals of the GPP-SIF relationship were analyzed to assess the potential use of VOD for estimating GPP. Residuals were calculated using a linear regression model following Guanter et al. (2014) and Damm et al. (2015). The regression models were evaluated for each grid cell separately with SIF as predictor variable. For grid cells with a significant regression ($p<0.05$), residuals were obtained as the difference between the observed and the SIF-

based estimate of GPP.

In addition to temporal correlations, spatial correlations were calculated to assess the similarity between maps. Since the spatial data were not normally distributed ($p>0.05$), Spearman rank correlation was used.

3. Results

3.1. Global patterns of VOD, GPP and SIF

Temporal median values of VOD, GPP and SIF reveal similar spatial patterns (Figure 1a-g), although spatial coverage of SMOS is reduced due to RFI masking. The spatial agreement with GPP is highest for SIF ($r=0.87$), followed by the passive VOD data sets ($0.73<r<0.79$) and is lowest for ASCAT ($r=0.47$). In general, regions of high VOD, i.e. high biomass, coincide with highly productive regions, which are primarily located in the tropics. In addition, high values are also found at high latitudes. In these regions, data masking due to low temperature and snow results in wintertime data gaps, which in turn increases temporal median values as they represent medians over the growing season only. Nevertheless, these relatively high values of productivity or VOD at high latitudes are mainly consistent across data sets.

Considering the absolute values of the VOD data, the data range differs between the data sets, which relates on the one hand to differences in the retrieval algorithm and version number and on the other hand to differences in sensor frequency. Since the focus of this study, however, is the temporal agreement between the data sets, differences in the absolute values were not

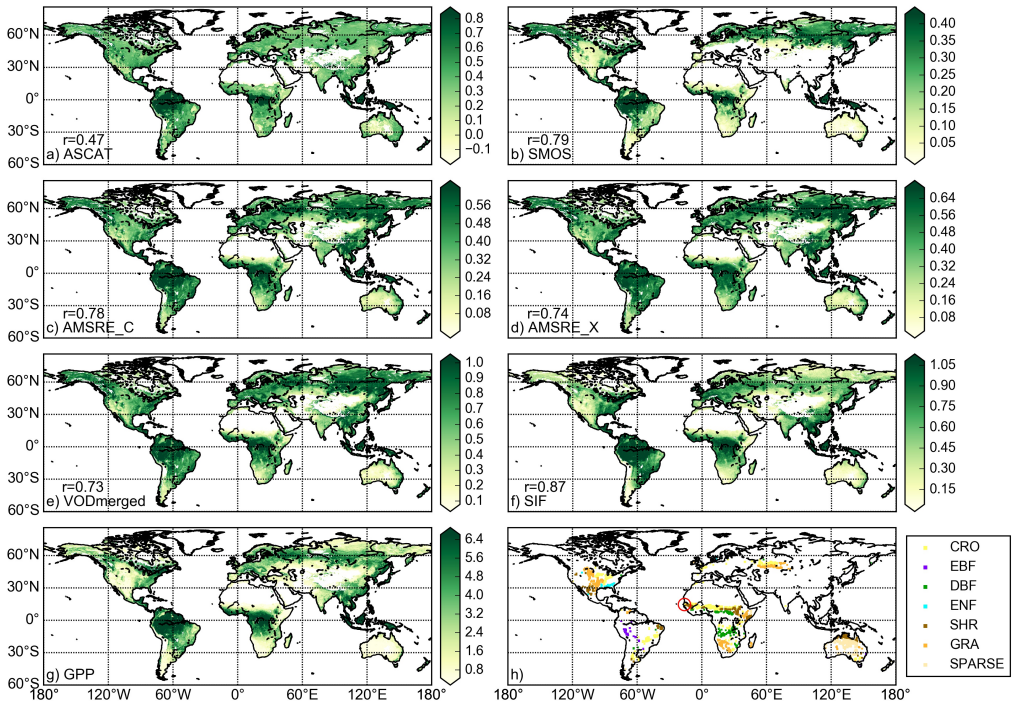

Figure 1: (a-g) Temporal median value of VOD data sets (a-e), SIF (f) and GPP (g). VOD is dimensionless, GPP is in $gCm^{-2}d^{-1}$ and SIF in $mWm^{-2}nm^{-1}sr^{-1}$. For visualization purposes, each data set is scaled between the 5th and the 95th percentile. (a-f) r denotes the spatial Spearman rank correlation between maps of temporal medians of GPP and VOD or SIF. All coefficients are highly significant ($p<0.001$). (h) Map of CCI land cover grid cells with a dominant land cover over 75% that correspond to the analyzed grid cells in Figure 4. The center of the red circle marks the location of the grid cell shown in Figure 8. Note that the size of the grid cells is enhanced for clearer visibility.

further analyzed.

Global temporal correlations between the original VOD time series and GPP at lag zero reveal positive agreement across large areas (Figure 2a-e). However, also some regions with negative correlations are observed. For ASCAT, negative correlations are found in Central America, South America, Africa and Southeast Asia. The passive VOD data sets show negative corre-

lations mainly in South America (in particular in the Amazon) and Southeast Asia. Although the results for different passive VOD data sets are similar in most areas, deviations from this behavior are found for SMOS and the merged VOD. For SMOS, negative correlations in central Africa coincide with those for ASCAT. For the merged VOD, predominantly positive correlations with GPP are observed in the Amazon, which contrasts with the negative values found for the other passive VOD data sets and may be related to differences in the algorithm version. Compared to the VOD data sets, the correlation between GPP and SIF (Figure 2f) is positive everywhere and on average much stronger. Nevertheless, also regions with no significant correlations ($p>0.05$) occur, which are mainly located in the tropics and in Australia. In the tropics, both GPP and SIF exhibit low variability, while the opposite, i.e. high variability for both data sets, is found in Australia (Figure S2).

Correlations between the anomalies of VOD and GPP (Figure 3a-e) also exhibit predominantly positive correlations. On average, the correlations are lower in magnitude than for the original time series but also show a lower number of negative values. Regions with relatively high correlations for the anomalies coincide with regions of high temporal agreement for the original time series, while some regions with negative correlations for the original time series result in no significant correlations for the anomalies. Highest correlation coefficients are observed in Australia. The correlations for the anomalies of GPP and SIF (Figure 3f) are of similar strength as the

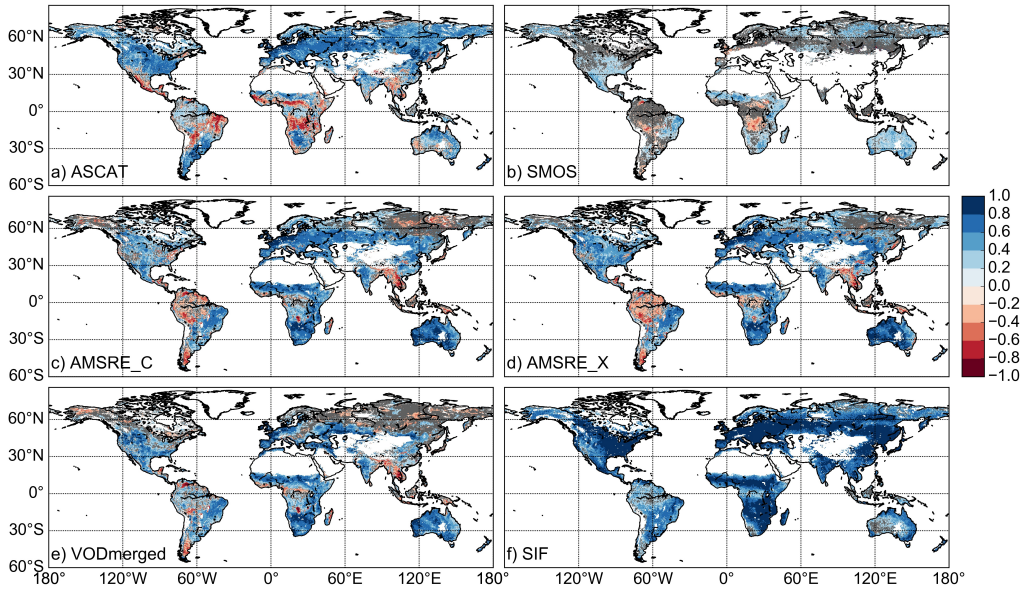

Figure 2: (a-e) Spearman rank correlation between GPP and VOD data sets at 0.25° and 8-daily resolution. Correlations that are not significant (p>0.05) are masked in grey. Corresponding correlations at 0.5° and monthly resolution are displayed in Figure S4. (f) Spearman rank correlation between GPP and SIF at 0.5° and monthly resolution.

correlations between the anomalies of GPP and VOD.

3.2. Temporal agreement with respect to SIF

The direct comparison of correlations between VOD and either GPP or SIF at homogeneous grid points (Figure 4) shows that the temporal agreement between VOD and SIF is similar to that found between VOD and GPP. In most cases, however, the median correlation coefficient is lower for the correlation between VOD and SIF than between VOD and GPP. This is especially pronounced for sparsely vegetated grid cells, which are mostly located in Australia (see Figure 1h).

In order to assess if VOD can provide additional information about GPP

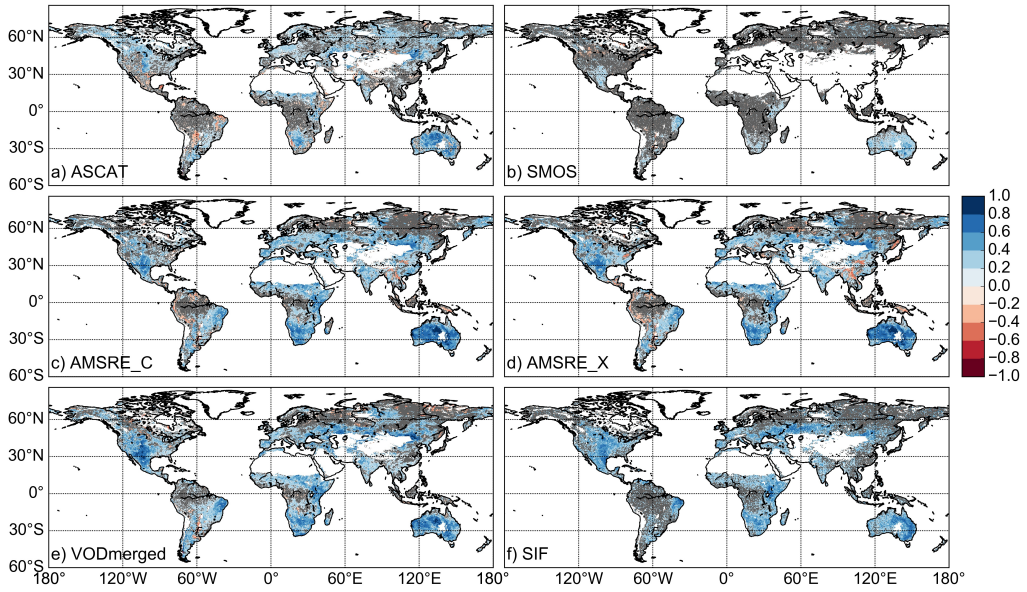

Figure 3: As Figure 2 but for the anomalies from the mean seasonal cycle. For a-e, the corresponding correlations at 0.5˚ and monthly resolution are shown in Figure S5.

on top of that provided by SIF, VOD was correlated with the residuals of the GPP-SIF relationship (Figure 5). The spatial maps reveal mainly positive correlations with negative correlations in the same areas as for the original time series but show a larger number of not significant correlations. In those areas where correlations are significant, VOD can explain variations in GPP that are not expressed through SIF using linear regression.

3.3. Comparison of the three variables for relating VOD to GPP

For the comparison of the three variables with GPP, only grid cells that resulted in significant correlations for all three variables are shown in Figure 6. For shrub-, crop-, grassland and sparse vegetation, all three variables yielded consistent, mainly positive correlations. Median values are generally lowest

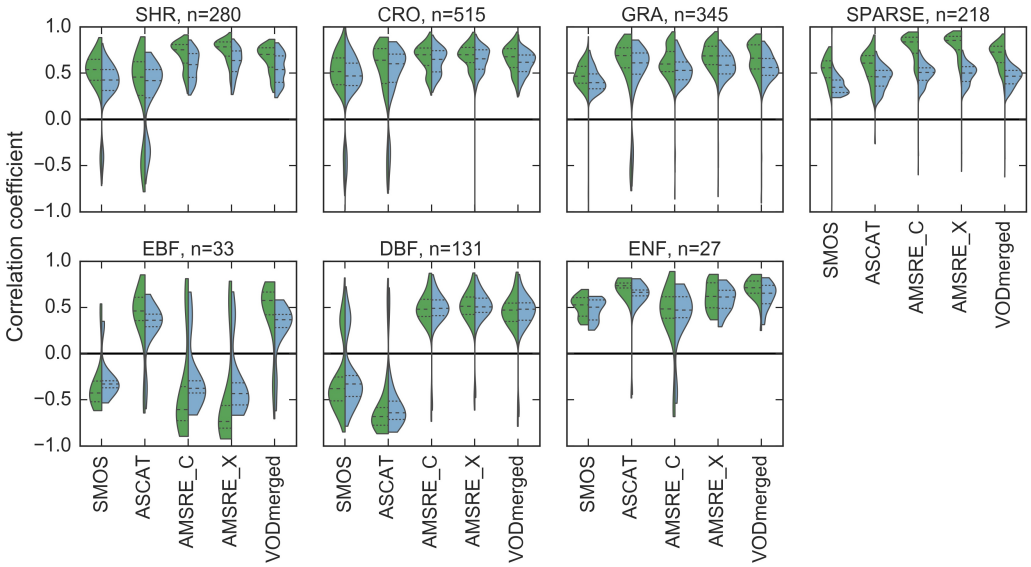

Figure 4: Violin plots of Spearman rank correlation between VOD and GPP (green) and between VOD and SIF (blue) at 0.5° and monthly resolution for grid cells with a dominant land cover fraction above 75%. Results are grouped according to the CCI land cover classification and single frequency data sets are ordered along increasing microwave frequency. The number of grid cells (n) is displayed above each graph. Horizontal lines within the violins indicate quartiles. Values that are not significant ($p>0.05$) are excluded. For the description of the land cover abbreviations see Table 2, for the spatial distribution of grid cells see Figure 1h. Note that DNF is not displayed since the analysis did not result in significant correlations for this land cover type.

for the correlation between SMOS and GPP and appear to increase with sensor frequency. In most cases, the original VOD time series result in higher median correlations with GPP than the changes in VOD. Highest median correlations are observed for shrubland for both frequencies of AMSR-E. Comparing the changes in VOD, results show that $\Delta\text{VOD}_{\geq 0}$ generally leads to higher correlations than ΔVOD.

For forests, results are not as consistent as for the sparsely to moderately vegetated areas. Nevertheless, forests also show on average a lower magnitude

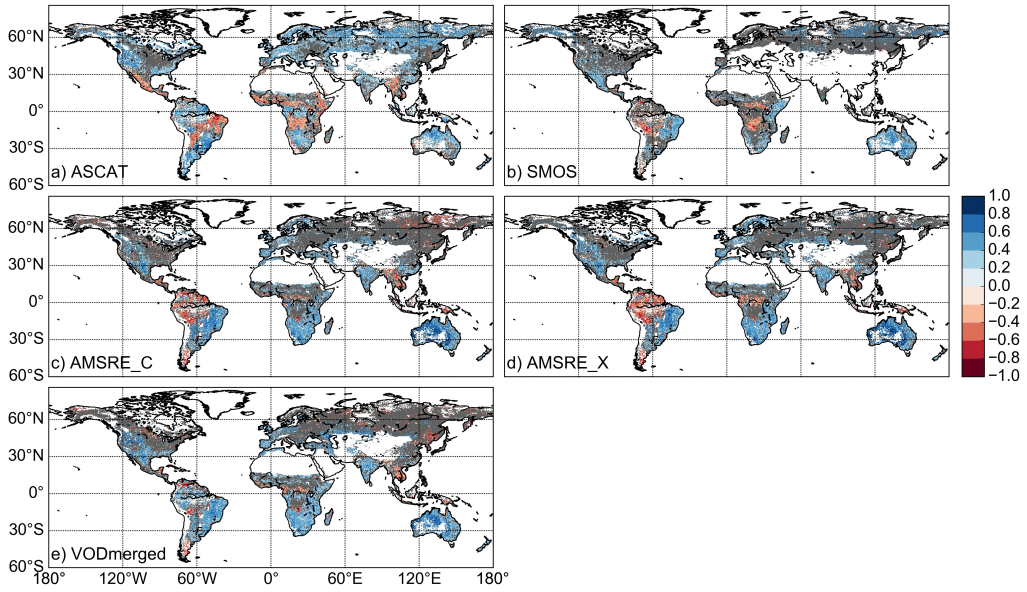

Figure 5: As Figure 2a-e but for the correlation between VOD and the residuals of the GPP-SIF relationship at 0.5° and monthly resolution.

of correlation between SMOS and GPP than for the remaining VOD data sets. Similar as for the sparsely to moderately vegetated areas, evergreen needleleaf forests exhibit generally higher correlations for the original VOD time series than for ΔVOD and $\Delta\text{VOD}_{\geq 0}$. In contrast, deciduous forests mainly yield higher median correlations for ΔVOD and $\Delta\text{VOD}_{\geq 0}$ than for the original VOD time series. Evergreen broadleaf forests, which exhibit low signal variability (see Figure S2) and a high number of negative correlations, do not show a consistent pattern for the three variables. Comparing only the changes in VOD for all forests, median correlations tend to be higher for ΔVOD than for $\Delta\text{VOD}_{\geq 0}$ and thus show the opposite behavior as for the sparsely to moderately vegetated areas.

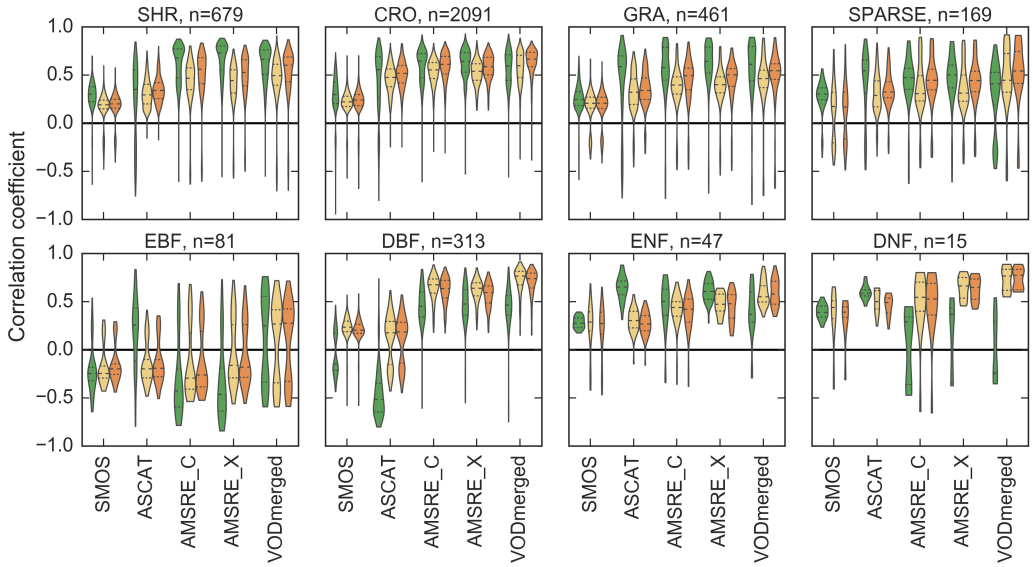

Figure 6: Violin plots of Spearman rank correlation between GPP and VOD (green), ΔVOD (yellow) or $\Delta\text{VOD}_{\geq 0}$ (orange) at 0.25° and 8-daily resolution. Results are displayed for grid cells with a dominant land cover fraction above 75% and grouped according to land cover (Table 2). n is the number of grid cells. Horizontal lines within the violins indicate quartiles. Values that are not significant ($p>0.05$) are excluded. See Figure S3 for the spatial map of the analyzed grid cells.

The spatial distributions of the correlations between GPP and the three VOD variables (Figures 2, S6 and S7) tend to complement each other. For grid points where the original VOD time series results in high correlations, ΔVOD and $\Delta\text{VOD}_{\geq 0}$ have lower correlations and vice versa. Since ΔVOD and $\Delta\text{VOD}_{\geq 0}$ both represent changes in VOD, their spatial correlation patterns with GPP are more similar compared to the correlation pattern between original VOD time series and GPP (Table S2).

The lag analysis (Figure 7) is based on the same grid cells as in Figure 6. On average, the original VOD time series follow the GPP signal: changes in GPP are reflected with some delay by subsequent changes of the VOD signal.

Apart from the broadleaf forests, all land cover classes exhibit median lag values ranging between 0 and 50 days. For ASCAT in deciduous broadleaf forest, the half a year's lag corresponds to the strong negative correlations found before for the zero-lagged correlations (Figure 6). In contrast to the positive lag found for the original VOD time series, the lag values for ΔVOD and $\Delta\text{VOD}_{\geq 0}$ are negative, which indicates that changes in VOD generally precede the GPP signal. In some cases, as for example in the deciduous broadleaf forest for AMSRE_C, AMSRE_X and the merged VOD, the absolute value of the median lag is smaller for ΔVOD and $\Delta\text{VOD}_{\geq 0}$ than for the original VOD time series. In these cases, calculating the change in VOD leads to a closer temporal agreement with GPP, which corresponds to the higher correlation coefficients found for the zero-lagged correlations.

This shift from positive to negative lag values for the different variables is further illustrated in Figure 8 for a rainfed cropland-dominated grid cell. Comparing the data close to the seasonal peaks, the original VOD time series decrease slower than the GPP signal, resulting in a positive lag (Figure 8b). For ΔVOD, the signal rises earlier than for GPP, which yields a negative lag (Figure 8c). Apart from the opposite sign of the lag value, the scaled ΔVOD signal shows a different shape than the GPP signal. ΔVOD exhibits a high number of values around 0.5, which represent ΔVOD values close to zero and are a result of the relatively long period of small changes in VOD. In this case, considering only positive changes in VOD appears to result in a higher temporal matching with GPP (Figure 8d), which explains the higher cor-

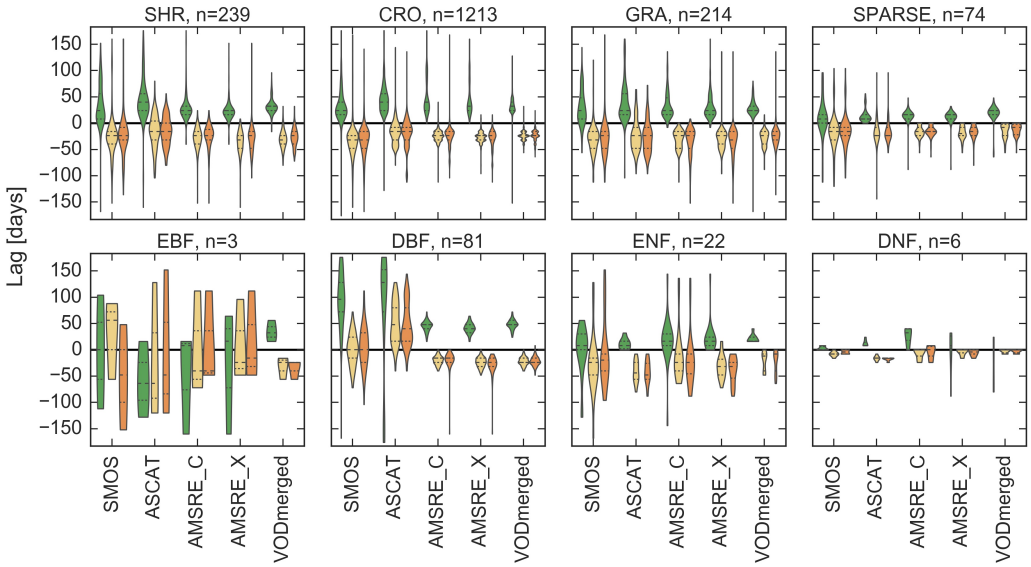

Figure 7: As Figure 6 but for the lag. Lag values are excluded if the lag is larger than half a year or the correlation of the lagged time series is not significant ($p>0.05$).

relations found for $\Delta VOD_{\geq 0}$ compared to ΔVOD in sparsely to moderately vegetated areas (Figure 6). Despite the overall higher temporal agreement for $\Delta VOD_{\geq 0}$ than for ΔVOD, the decline in GPP is better captured by ΔVOD.

The relationships between the three VOD variables and GPP can be further assessed with the corresponding scatter plots (Figures 8e-g). This relationship describes a seasonal hysteresis. Comparing all three variables, the shape of the mean seasonal cycle appears to be similar for the original VOD time series and ΔVOD as they both exhibit a pronounced linear part, while this feature is missing for $\Delta VOD_{\geq 0}$. The linear part for the original VOD, however, corresponds to the GPP increase, while for ΔVOD the linear part relates to the GPP decrease.

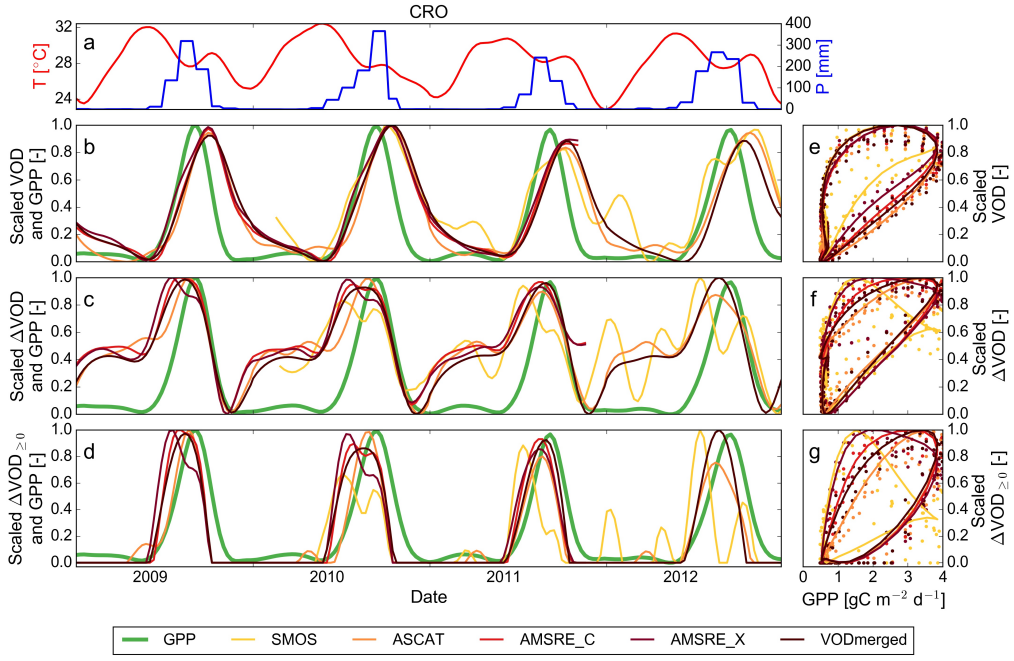

Figure 8: Time series (a-d) and scatter plots (e-g) at 8-daily resolution for a cropland-dominated grid cell in West Sahel, located at 16.125W 14.625N, for the period 2009-2012 (location is indicated in Figure 1f). (a) Skin temperature (T) and monthly sums of precipitation (P). (b-d) VOD (b), ΔVOD (c), or $\Delta\text{VOD}_{\geq 0}$ (d) together with GPP. Data are smoothed and scaled between their minimum and maximum for visualization purposes. Note that the unscaled ΔVOD includes negative values. (e-g) Scatter plots of scaled VOD variables against unscaled GPP for the same data as in (b-d).

4. Discussion

4.1. Temporal agreement between VOD, GPP and SIF

In this study, large parts of the world reveal positive correlations between VOD and GPP both for the original time series and for the anomalies from the mean seasonal cycle. In addition, correlations between VOD and the residuals of the linear GPP-SIF relationship demonstrate that VOD can explain variations in GPP that are not explained by SIF. These findings

suggests that VOD provides useful information with regard to GPP.

Water limitation appears to foster the coupling between VOD and GPP as areas with particularly high correlations between VOD and GPP in this study seem to coincide with areas of low water availability (Miralles et al., 2016; Papagiannopoulou et al., 2017). In these areas, vegetation responds more rapidly to changes in water availability (De Keersmaecker et al., 2015), which in turn is reflected in a close association between VOD and GPP.

The most prominent example of low correlations in this study is found for evergreen broadleaf forests, which can be attributed to the low signal variability found in the tropics. This is in line with the generally low predictability of GPP in tropical forests (Tramontana et al., 2016) and can be linked to isohydricity, which describes the plant strategy of stomatal control in response to water stress (Konings and Gentine, 2016). Evergreen broadleaf forests are very isohydric, i.e. they try to minimize changes in leaf water potential by closing stomata (Fisher et al., 2006; Konings and Gentine, 2016). This closing of stomata may result in a decoupling of VWC and photosynthetic activity and hence cause a weaker relationship between VOD and GPP.

4.2. Occurrence of negative correlations between VOD and GPP

Negative correlations between VOD and GPP can be attributed to land surface properties and vegetation phenology. For ASCAT, negative correlations can be explained with the contribution of dry soil to volume scattering (Vreugdenhil et al., 2016a), which is often found for ASCAT backscatter in

arid and semi-arid regions (Wagner et al., 2013b; De Jeu et al., 2008). Liu et al. (2016) showed for L-band backscatter that the scattering mechanism of the soil shifts from surface scattering under wet conditions to volume scattering under very dry conditions; below a certain soil moisture threshold, the backscatter increases again with decreasing soil moisture. Some grid cells showing negative correlations are found in the tropical dry forest biome, which regularly experience a pronounced dry season lasting up to six months (Olivares and Medina, 1992). Therefore, depending on the duration and severity of the seasonal dry period and on the soil properties, volume scattering of dry soil might lead to spurious signals in the VOD if soil volume scattering is not taken into account in the retrieval algorithm, as is the case for the ASCAT TU-Wien algorithm (Hahn et al., 2017).

In contrast to the active VOD, most negative correlations for passive VOD data can be linked to wetlands (Jones et al., 2011; Liu et al., 2011; Vreugdenhil et al., 2016b). Jones et al. (2011) demonstrated that passive VOD data exhibit an inverse relationship with vegetation growth for areas that are seasonally inundated.

For evergreen broadleaf forest, negative correlations with GPP for SMOS, AMSRE_C, and AMSRE_X may partly relate to leaf phenology. Jones et al. (2014) reported asynchronous behavior between flux tower GPP estimates and AMSR-E C-band VOD for the Amazon forest, which may be linked to an inverse relationship between leaf age and photosynthetic capacity. New leaves, which flush during the dry season (Wright and van Schaik, 1994; Huete

et al., 2006), are photosynthetically more active than old leaves (Kitajima et al., 2002; Hutyra et al., 2007) but may also cause overall lower values of VOD.

Similarly, negative correlations found for SMOS in Africa may relate to the phenology in tropical dry forests. Early studies demonstrated that deciduous trees in dry forests minimize their water loss by leaf shedding, and that some trees also flower during the dry season or often leaf out at the end of the dry season (Olivares and Medina, 1992; Borchert, 1994a,b). In terms of the VOD signal, this means that trunks and branches still contain a relatively high amount of water during the dry season. Since L-band data is most sensitive to larger structures (Woodhouse, 2005), this asynchronous behavior of the stem water content may lead to the observed negative correlations between SMOS and GPP.

4.3. Effect of sensor frequency

The comparison of different sensor frequencies between 1 and 10 GHz (L-, C-, and X-band) showed that for sparsely to moderately vegetated areas median correlations increased with sensor frequency. In line with this result, Calvet et al. (2011) demonstrated for a dense wheat field that C- and X-band microwave observations obtained from a ground-based radiometer are more sensitive to VWC than L-band data. Since VWC is linearly related to VOD (Jackson and Schmugge, 1991; Woodhouse, 2005), this can explain the lower magnitude of the correlation coefficients between SMOS and GPP

compared to the remaining VOD data sets. For forested regions, a similar behavior, with a low magnitude of the correlation for SMOS, was observed in this study. This suggests that C- and X-band microwave observations are better suited for relating VOD to GPP than L-band data.

4.4. Comparison of the three VOD variables in relation to GPP

Detailed knowledge about land cover is of decisive importance when assessing VOD in relation to GPP. Large differences exist for the three VOD variables between forested and non-forested regions. While ΔVOD shows a higher temporal agreement with GPP over forests, the original VOD time series yield higher correlations with GPP for sparsely to moderately vegetated areas.

According to the lag analysis, all three VOD variables generally did not yield a zero lag. The opposite signs for VOD compared to ΔVOD and $\Delta\text{VOD}_{\geq 0}$ suggest that at the global scale neither the original VOD time series nor the changes in VOD alone can be used for relating VOD to GPP, but instead should be combined. The reason why both VOD and ΔVOD (or $\Delta\text{VOD}_{\geq 0}$) are linked to GPP, i.e. the sum of NPP and autotrophic respiration, can be explained with the contribution of both biomass and growth-related terms to GPP.

NPP relates to the sum of above- and belowground NPP as well as losses through volatile organic compounds (VOC), herbivory and root exudates (Clark et al., 2001a,b; Gower et al., 2001; Girardin et al., 2010). Assuming

that belowground NPP is a fraction of ANPP (Clark et al., 2001a), these two terms relate to changes in biomass and, hence, to ΔVOD. The magnitude of the VOC flux was estimated to be small compared to NPP or GPP (Guenther et al., 1995; Kesselmeier et al., 2002), and losses through herbivory between consecutive observations and root exudates are difficult to quantify.

Autotrophic respiration can be expressed as the sum of maintenance and growth respiration; while maintenance respiration is proportional to living biomass, growth respiration is a function of the change in biomass (Ryan, 1990; Lavigne et al., 1996). Hence, VOD and ΔVOD can be related to maintenance and growth respiration, respectively. This suggests that GPP may be expressed as a combination of VOD and ΔVOD.

The relationship between VOD, ΔVOD or $\Delta VOD_{\geq 0}$ and GPP may also vary throughout the season leading to hysteresis as shown in this study for a cropland-dominated grid cell. Similarly, but for the relationship between LAI and GPP, Gitelson et al. (2014) emphasized the importance of seasonal hysteresis. In the current study, the hysteresis was also present for ΔVOD, which indicates that this behavior is not merely a result of using a state (VOD) rather than a flux variable (ΔVOD). The presence of a seasonal hysteresis also explains here the on average lower correlations found for GPP vs VOD compared to GPP vs SIF, since such a hysteresis decreases the strength of the linear relationship. Combining the original VOD time series and the change in VOD thus might reduce the strength of the seasonal hysteresis and thereby improve the temporal agreement with GPP.

5. Conclusions

The global analysis of VOD from different frequencies (L-, C- and X-band) in relation to GPP indicates that microwave VOD, which provides complementary information to optical data, has the potential to serve as explanatory variable for estimating GPP. Although some negative correlations occurred in dry and wet areas for active and passive VOD, respectively, VOD and changes in VOD (ΔVOD or $\Delta VOD_{\geq 0}$) generally demonstrated a high temporal agreement with GPP, especially for C- and X-band data. The mainly non-overlapping distributions of negative correlations for active and passive observations indicate that active and passive VOD data should be used jointly. Land cover based differences in lag and correlation coefficient further suggest to combine original VOD time series with changes in VOD for relating VOD to GPP. In addition, seasonal hysteresis was observed for the relationship between VOD variables and GPP, which demonstrates that this relationship may vary both in space and in time. This underpins the need to further investigate the spatio-temporal relationship between VOD and GPP in order to make full use of microwave satellite vegetation data for regional to global ecosystem analyses and vegetation monitoring.

6. Acknowledgements

The study is performed as part of the EOWAVE project funded by the TU Wien Wissenschaftspreis 2015 awarded to Wouter Dorigo by the Vienna University of Technology (http://climers.geo.tuwien.ac.at/) with con-

tributions of the STR3S project funded by the Belgian Science Policy Office (BELSPO) as part of the STEREO III program. D G Miralles acknowledges support from the European Research Council (ERC) under grant agreement n°715254 (DRY–2–DRY).

References

Andela, N., Liu, Y. Y., van Dijk, A. I. J. M., de Jeu, R. A. M., McVicar, T. R., 2013. Global changes in dryland vegetation dynamics (1988-2008) assessed by satellite remote sensing: comparing a new passive microwave vegetation density record with reflective greenness data. Biogeosciences 10 (10), 6657–6676.
URL http://www.biogeosciences.net/10/6657/2013/

Baldocchi, D., Falge, E., Gu, L., Olson, R., Hollinger, D., Running, S., Anthoni, P., Bernhofer, C., Davis, K., Evans, R., Fuentes, J., Goldstein, A., Katul, G., Law, B., Lee, X., Malhi, Y., Meyers, T., Munger, W., Oechel, W., Paw, K. T., Pilegaard, K., Schmid, H. P., Valentini, R., Verma, S., Vesala, T., Wilson, K., Wofsy, S., 2001. FLUXNET: A New Tool to Study the Temporal and Spatial Variability of Ecosystem–Scale Carbon Dioxide, Water Vapor, and Energy Flux Densities. Bulletin of the American Meteorological Society 82 (11), 2415–2434.
URL http://journals.ametsoc.org/doi/abs/10.1175/1520-0477(2001)0823C2415:FANTTS3E2.3.CO;2

Beer, C., Reichstein, M., Tomelleri, E., Ciais, P., Jung, M., Carvalhais, N., Rödenbeck, C., Arain, M. A., Baldocchi, D., Bonan, G. B., Bondeau, A., Cescatti, A., Lasslop, G., Lindroth, A., Lomas, M., Luyssaert, S., Margolis, H., Oleson, K. W., Roupsard, O., Veenendaal, E., Viovy, N., Williams, C., Woodward, F. I., Papale, D., 2010. Terrestrial Gross Carbon Dioxide Uptake: Global Distribution and Covariation with Climate. Science 329 (5993), 834–838.
URL http://science.sciencemag.org/content/329/5993/834

Bonan, G., 2015. Ecological Climatology: Concepts and Applications.
URL https://books.google.at/books/about/Ecological_Climatology.html?id=kq8kDQAAQBAJ

Bonan, G. B., 2008. Forests and Climate Change: Forcings, Feedbacks, and the Climate Benefits of Forests. Science 320 (5882), 1444–1449.
URL http://science.sciencemag.org/content/320/5882/1444

Bontemps, S., Defourny, P., Radoux, J., Van Bogaert, E., Lamarche, C., Achard, F., Mayaux, P., Boettcher, M., Brockmann, C., Kirches, G., Zülkhe, M., Kalogirou, V., Seifert, F. M., Arino, O., 2013. Consistent global land cover maps for climate modelling communities: current achievements of the ESA' Land cover CCI. In: ESA Living Planet Symposium 2013. Edinburgh, UK.
URL https://ftp.space.dtu.dk/pub/Ioana/papers/s274_2bont.pdf

Borchert, R., 1994a. Soil and Stem Water Storage Determine Phenology and

Distribution of Tropical Dry Forest Trees. Ecology 75 (5), 1437–1449.
URL http://onlinelibrary.wiley.com/doi/10.2307/1937467/abstract

Borchert, R., 1994b. Water status and development of tropical trees during seasonal drought. Trees 8 (3), 115–125.
URL http://link.springer.com/article/10.1007/BF00196635

Calvet, J.-C., Wigneron, J.-P., Walker, J., Karbou, F., Chanzy, A., Albergel, C., 2011. Sensitivity of Passive Microwave Observations to Soil Moisture and Vegetation Water Content: L-Band to W-Band. IEEE Transactions on Geoscience and Remote Sensing 4 (49), 1190–1199.
URL https://www.infona.pl//resource/bwmeta1.element.ieee-art-000005492186

Campioli, M., Gielen, B., Göckede, M., Papale, D., Bouriaud, O., Granier, A., 2011. Temporal variability of the NPP-GPP ratio at seasonal and interannual time scales in a temperate beech forest. Biogeosciences 8 (9), 2481–2492.
URL http://www.biogeosciences.net/8/2481/2011/

Campioli, M., Malhi, Y., Vicca, S., Luyssaert, S., Papale, D., Peñuelas, J., Reichstein, M., Migliavacca, M., Arain, M. A., Janssens, I. A., 2016. Evaluating the convergence between eddy-covariance and biometric methods for assessing carbon budgets of forests. Nature Communications

640 7, 13717.
641 URL http://www.nature.com/ncomms/2016/161214/ncomms13717/
642 full/ncomms13717.html

643 Chen, J., Jönsson, P., Tamura, M., Gu, Z., Matsushita, B., Eklundh,
644 L., 2004. A simple method for reconstructing a high-quality NDVI
645 time-series data set based on the Savitzky–Golay filter. Remote Sensing
646 of Environment 91 (3–4), 332–344.
647 URL http://www.sciencedirect.com/science/article/pii/
648 S003442570400080X

649 Ciais, P., Sabine, C., Bala, G., Bopp, L., Brovkin, V., Canadell, J., Chhabra,
650 A., DeFries, R., Galloway, J., Heimann, M., Jones, C., Le Quéré, C., My-
651 neni, R. B., Piao, S., Thornton, P., 2013. Carbon and Other Biogeochem-
652 ical Cycles. In: Stocker, T., Qin, D., Plattner, G.-K., Tignor, M., Allen,
653 S., Boschung, J., Nauels, A., Xia, Y., Bex, V., Midgley, P. (Eds.), Climate
654 Change 2013: The Physical Science Basis. Contribution of Working Group
655 I to the Fifth Assessment Report of the Intergovernmental Panel on Cli-
656 mate Change. Cambridge University Press, Cambridge, United Kingdom
657 and New York, NY, USA.

658 Clark, D. A., Brown, S., Kicklighter, D. W., Chambers, J. Q., Thomlinson,
659 J. R., Ni, J., 2001a. Measuring net primary production in forests:
660 Concepts and field methods. Ecological Applications 11 (2), 356–370.

661 URL http://onlinelibrary.wiley.com/doi/10.1890/
662 1051-0761(2001)011[0356:MNPPIF]2.0.CO;2/abstract

663 Clark, D. A., Brown, S., Kicklighter, D. W., Chambers, J. Q., Thomlinson,
664 J. R., Ni, J., Holland, E. A., 2001b. Net Primary Production in Tropical
665 Forests: An Evaluation and Synthesis of existing field data. Ecological
666 Applications 11 (2), 371–384.
667 URL ftp://ftp.forest.sr.unh.edu/pub/MLSmith/John20R/Backup/
668 NPP,carbon20pub/i1051-0761-011-02-0371.pdf

669 Collatz, G. J., Ribas-Carbo, M., Berry, J. A., Collatz, G. J., Ribas-Carbo, M.,
670 Berry, J. A., 1992. Coupled Photosynthesis-Stomatal Conductance Model
671 for Leaves of C4 Plants, Coupled Photosynthesis-Stomatal Conductance
672 Model for Leaves of C4 Plants. Functional Plant Biology 19 (5), 519–538.
673 URL http://www.publish.csiro.au/fp/PP9920519

674 D'Agostino, R., Pearson, E. S., 1973. Tests for departure from normality.
675 Empirical results for the distributions of b2 and $\sqrt{\text{b1}}$. Biometrika 60 (3),
676 613–622.
677 URL http://biomet.oxfordjournals.org/content/60/3/613

678 D'Agostino, R. B., 1971. An omnibus test of normality for moderate and
679 large size samples. Biometrika 58 (2), 341–348.
680 URL http://biomet.oxfordjournals.org/content/58/2/341

681 Damm, A., Guanter, L., Paul-Limoges, E., van der Tol, C., Hueni, A.,

Buchmann, N., Eugster, W., Ammann, C., Schaepman, M. E., 2015. Far-red sun-induced chlorophyll fluorescence shows ecosystem-specific relationships to gross primary production: An assessment based on observational and modeling approaches. Remote Sensing of Environment 166, 91–105.
URL http://www.sciencedirect.com/science/article/pii/S0034425715300341

De Jeu, R. A. M., Wagner, W., Holmes, T. R. H., Dolman, A. J., Giesen, N. C. v. d., Friesen, J., 2008. Global Soil Moisture Patterns Observed by Space Borne Microwave Radiometers and Scatterometers. Surveys in Geophysics 29 (4-5), 399–420.
URL http://link.springer.com/article/10.1007/s10712-008-9044-0

De Keersmaecker, W., Lhermitte, S., Tits, L., Honnay, O., Somers, B., Coppin, P., 2015. A model quantifying global vegetation resistance and resilience to short-term climate anomalies and their relationship with vegetation cover: Global vegetation resistance and resilience. Global Ecology and Biogeography 24 (5), 539–548.
URL http://doi.wiley.com/10.1111/geb.12279

Dee, D. P., Uppala, S. M., Simmons, A. J., Berrisford, P., Poli, P., Kobayashi, S., Andrae, U., Balmaseda, M. A., Balsamo, G., Bauer, P., Bechtold, P., Beljaars, A. C. M., van de Berg, L., Bidlot, J., Bormann,

N., Delsol, C., Dragani, R., Fuentes, M., Geer, A. J., Haimberger, L., Healy, S. B., Hersbach, H., Hólm, E. V., Isaksen, L., Kållberg, P., Köhler, M., Matricardi, M., McNally, A. P., Monge-Sanz, B. M., Morcrette, J.-J., Park, B.-K., Peubey, C., de Rosnay, P., Tavolato, C., Thépaut, J.-N., Vitart, F., 2011. The ERA-Interim reanalysis: configuration and performance of the data assimilation system. Quarterly Journal of the Royal Meteorological Society 137 (656), 553–597.
URL http://onlinelibrary.wiley.com/doi/10.1002/qj.828/abstract

Dorigo, W. A., 2012. Improving the Robustness of Cotton Status Characterisation by Radiative Transfer Model Inversion of Multi-Angular CHRIS/PROBA Data. IEEE Journal of Selected Topics in Applied Earth Observations and Remote Sensing 5 (1), 18–29.

Dorigo, W. A., Gruber, A., De Jeu, R. A. M., Wagner, W., Stacke, T., Loew, A., Albergel, C., Brocca, L., Chung, D., Parinussa, R. M., Kidd, R., 2015. Evaluation of the ESA CCI soil moisture product using ground-based observations. Remote Sensing of Environment 162, 380–395.
URL http://www.sciencedirect.com/science/article/pii/S0034425714002727

Dorigo, W. A., Zurita-Milla, R., de Wit, A. J. W., Brazile, J., Singh, R., Schaepman, M. E., 2007. A review on reflective remote sensing and data assimilation techniques for enhanced agroecosystem modeling.

International Journal of Applied Earth Observation and Geoinformation 9 (2), 165–193.
URL http://www.sciencedirect.com/science/article/pii/S0303243406000201

Draper, C. S., Reichle, R. H., Lannoy, D., M, G. J., Liu, Q., 2012. Assimilation of passive and active microwave soil moisture retrievals. Geophysical Research Letters 39 (4).
URL http://onlinelibrary.wiley.com/doi/10.1029/2011GL050655/abstract

Farquhar, G. D., Caemmerer, S. v., Berry, J. A., 1980. A biochemical model of photosynthetic CO2 assimilation in leaves of C3 species. Planta 149 (1), 78–90.
URL http://link.springer.com/article/10.1007/BF00386231

Fisher, R. A., Williams, M., Vale, D., Lobo, R., Costa, D., Lola, A., Meir, P., 2006. Evidence from amazonian forests is consistent with isohydric control of leaf water potential 29 (2), 151–165.
URL http://onlinelibrary.wiley.com/doi/10.1111/j.1365-3040.2005.01407.x/full

Forkel, M., Carvalhais, N., Verbesselt, J., Mahecha, M. D., Neigh, C. S. R., Reichstein, M., 2013. Trend Change Detection in NDVI Time Series: Effects of Inter-Annual Variability and Methodology. Remote Sensing 5 (5),

747 2113–2144.

748 URL http://www.mdpi.com/2072-4292/5/5/2113

749 Frankenberg, C., O'Dell, C., Berry, J., Guanter, L., Joiner, J., Köhler, P.,
750 Pollock, R., Taylor, T. E., 2014. Prospects for chlorophyll fluorescence
751 remote sensing from the Orbiting Carbon Observatory-2. Remote Sensing
752 of Environment 147, 1–12.
753 URL http://linkinghub.elsevier.com/retrieve/pii/
754 S0034425714000522

755 Girardin, C. a. J., Malhi, Y., Aragão, L. E. O. C., Mamani, M.,
756 Huaraca Huasco, W., Durand, L., Feeley, K. J., Rapp, J., Silva-Espejo,
757 J. E., Silman, M., Salinas, N., Whittaker, R. J., 2010. Net primary
758 productivity allocation and cycling of carbon along a tropical forest
759 elevational transect in the Peruvian Andes. Global Change Biology
760 16 (12), 3176–3192.
761 URL http://onlinelibrary.wiley.com/doi/10.1111/j.1365-2486.
762 2010.02235.x/full

763 Gitelson, A. A., Peng, Y., Arkebauer, T. J., Schepers, J., 2014. Relationships
764 between gross primary production, green LAI, and canopy chlorophyll
765 content in maize: Implications for remote sensing of primary production.
766 Remote Sensing of Environment 144, 65–72.
767 URL http://www.sciencedirect.com/science/article/pii/
768 S0034425714000170

769 Gower, S. T., Krankina, O., Olson, R. J., Apps, M., Linder, S., Wang, C.,
770 2001. Net primary production and carbon allocation patterns of boreal
771 forest ecosystems. Ecological Applications 11 (5), 1395–1411.
772 URL http://onlinelibrary.wiley.com/doi/10.1890/
773 1051-0761(2001)011[1395:NPPACA]2.0.CO;2/full

774 Guanter, L., Zhang, Y., Jung, M., Joiner, J., Voigt, M., Berry, J. A., Franken-
775 berg, C., Huete, A. R., Zarco-Tejada, P., Lee, J.-E., Moran, M. S., Ponce-
776 Campos, G., Beer, C., Camps-Valls, G., Buchmann, N., Gianelle, D.,
777 Klumpp, K., Cescatti, A., Baker, J. M., Griffis, T. J., 2014. Global and
778 time-resolved monitoring of crop photosynthesis with chlorophyll fluores-
779 cence. Proceedings of the National Academy of Sciences 111 (14), E1327–
780 E1333.
781 URL http://www.pnas.org/content/111/14/E1327

782 Guenther, A., Hewitt, C. N., Erickson, D., Fall, R., Geron, C., Graedel, T.,
783 Harley, P., Klinger, L., Lerdau, M., Mckay, W. A., Pierce, T., Scholes,
784 B., Steinbrecher, R., Tallamraju, R., Taylor, J., Zimmerman, P., 1995. A
785 global model of natural volatile organic compound emissions. Journal of
786 Geophysical Research 100 (D5), 8873–8892.
787 URL http://doi.wiley.com/10.1029/94JD02950

788 Hahn, S., Reimer, C., Vreugdenhil, M., Melzer, T., Wagner, W., 2017. Dy-
789 namic Characterization of the Incidence Angle Dependence of Backscatter

790 Using Metop ASCAT. IEEE Journal of Selected Topics in Applied Earth
791 Observations and Remote Sensing PP (99), 1–12.

792 Holben, B. N., 1986. Characteristics of maximum-value composite images
793 from temporal AVHRR data. International Journal of Remote Sensing
794 7 (11), 1417–1434.
795 URL http://www.tandfonline.com/doi/abs/10.1080/
796 01431168608948945

797 Huete, A., Didan, K., Leeuwen, W. v., Miura, T., Glenn, E., 2011. MODIS
798 Vegetation Indices. In: Land Remote Sensing and Global Environmental
799 Change. pp. 579–602.
800 URL http://link.springer.com/chapter/10.1007/
801 978-1-4419-6749-7_26

802 Huete, A. R., Didan, K., Shimabukuro, Y. E., Ratana, P., Saleska, S. R.,
803 Hutyra, L. R., Yang, W., Nemani, R. R., Myneni, R., 2006. Amazon rain-
804 forests green-up with sunlight in dry season 33 (6).
805 URL http://onlinelibrary.wiley.com/doi/10.1029/2005GL025583/
806 full

807 Huffman, G. J., Adler, R. F., Morrissey, M. M., Bolvin, D. T., Curtis, S.,
808 Joyce, R., McGavock, B., Susskind, J., 2001. Global Precipitation at
809 One-Degree Daily Resolution from Multisatellite Observations. Journal of
810 Hydrometeorology 2 (1), 36–50.

URL http://journals.ametsoc.org/doi/full/10.1175/1525-7541(2001)0023C00363AGPAODD3E2.0.CO3B2

Hutyra, L. R., Munger, J. W., Saleska, S. R., Gottlieb, E., Daube, B. C., Dunn, A. L., Amaral, D. F., Camargo, D., B, P., Wofsy, S. C., 2007. Seasonal controls on the exchange of carbon and water in an amazonian rain forest 112.
URL http://onlinelibrary.wiley.com/doi/10.1029/2006JG000365/full

Jackson, T. J., Schmugge, T. J., 1991. Vegetation effects on the microwave emission of soils. Remote Sensing of Environment 36 (3), 203–212.
URL http://www.sciencedirect.com/science/article/pii/003442579190057D

Joiner, J., Guanter, L., Lindstrot, R., Voigt, M., Vasilkov, A. P., Middleton, E. M., Huemmrich, K. F., Yoshida, Y., Frankenberg, C., 2013. Global monitoring of terrestrial chlorophyll fluorescence from moderate-spectral-resolution near-infrared satellite measurements: methodology, simulations, and application to GOME-2. Atmospheric Measurement Techniques 6, 2803–2823.
URL http://www.atmos-meas-tech.net/6/2803/2013/amt-6-2803-2013.pdf

Joiner, J., Yoshida, Y., Guanter, L., Middleton, E. M., 2016. New methods for the retrieval of chlorophyll red fluorescence from hyperspectral satellite

instruments: simulations and application to GOME-2 and SCIAMACHY. Atmospheric Measurement Techniques 9 (8), 3939–3967.
URL http://www.atmos-meas-tech.net/9/3939/2016/amt-9-3939-2016-discussion.html

Joiner, J., Yoshida, Y., Vasilkov, A. P., Schaefer, K., Jung, M., Guanter, L., Zhang, Y., Garrity, S., Middleton, E. M., Huemmrich, K. F., Gu, L., Belelli Marchesini, L., 2014. The seasonal cycle of satellite chlorophyll fluorescence observations and its relationship to vegetation phenology and ecosystem atmosphere carbon exchange. Remote Sensing of Environment 152, 375–391.
URL http://www.sciencedirect.com/science/article/pii/S0034425714002429

Jones, M. O., Jones, L. A., Kimball, J. S., McDonald, K. C., 2011. Satellite passive microwave remote sensing for monitoring global land surface phenology. Remote Sensing of Environment 115 (4), 1102–1114.
URL http://www.sciencedirect.com/science/article/pii/S0034425710003615

Jones, M. O., Kimball, J. S., Jones, L. A., McDonald, K. C., 2012. Satellite passive microwave detection of North America start of season. Remote Sensing of Environment 123, 324–333.
URL http://www.sciencedirect.com/science/article/pii/S0034425712001575

Jones, M. O., Kimball, J. S., Nemani, R. R., 2014. Asynchronous Amazon forest canopy phenology indicates adaptation to both water and light availability. Environmental Research Letters 9 (12), 124021.
URL http://stacks.iop.org/1748-9326/9/i=12/a=124021?key=crossref.10b2710176d7cd3ad2f6d5d1d5fa1e07

Jung, M., Reichstein, M., Margolis, H. A., Cescatti, A., Richardson, A. D., Arain, M. A., Arneth, A., Bernhofer, C., Bonal, D., Chen, J., Gianelle, D., Gobron, N., Kiely, G., Kutsch, W., Lasslop, G., Law, B. E., Lindroth, A., Merbold, L., Montagnani, L., Moors, E. J., Papale, D., Sottocornola, M., Vaccari, F., Williams, C., 2011. Global patterns of land-atmosphere fluxes of carbon dioxide, latent heat, and sensible heat derived from eddy covariance, satellite, and meteorological observations. Journal of Geophysical Research 116 (G3), G00J07.
URL http://doi.wiley.com/10.1029/2010JG001566

Kesselmeier, J., Ciccioli, P., Kuhn, U., Stefani, P., Biesenthal, T., Rottenberger, S., Wolf, A., Vitullo, M., Valentini, R., Nobre, A., Kabat, P., Andreae, M. O., 2002. Volatile organic compound emissions in relation to plant carbon fixation and the terrestrial carbon budget. Global Biogeochemical Cycles 16 (4).
URL http://onlinelibrary.wiley.com/doi/10.1029/2001GB001813/full

Kim, Y., Jackson, T., Bindlish, R., Lee, H., Hong, S., 2012. Radar Vegetation

877 Index for Estimating the Vegetation Water Content of Rice and Soybean.
878 IEEE Geoscience and Remote Sensing Letters 9 (4), 564–568.

879 Kitajima, K., Mulkey, S. S., Samaniego, M., Wright, S. J., 2002. Decline of
880 photosynthetic capacity with leaf age and position in two tropical pioneer
881 tree species 89 (12), 1925–1932.
882 URL http://www.amjbot.org/content/89/12/1925

883 Kokoska, S., Zwillinger, D., 2000. CRC Standard Probability and Statis-
884 tics Tables and Formulae, Student Edition. CRC Press, google-Books-ID:
885 G5hJqwjweiUC.

886 Konings, A. G., Gentine, P., 2016. Global variations in ecosystem-scale iso-
887 hydricity. Global Change Biology 23 (2), 891–905.
888 URL http://doi.wiley.com/10.1111/gcb.13389

889 Lambers, H., Chapin, F. S. I., Pons, T. L., 2008. Plant Physiological Ecology.
890 Springer Science & Business Media.
891 URL https://books.google.at/books/about/Plant_Physiological_
892 Ecology.html?hl=de&id=PXBq6jsT5SYC

893 Lasslop, G., Migliavacca, M., Bohrer, G., Reichstein, M., Bahn, M., Ibrom,
894 A., Jacobs, C., Kolari, P., Papale, D., Vesala, T., Wohlfahrt, G., Cescatti,
895 A., 2012. On the choice of the driving temperature for eddy-covariance
896 carbon dioxide flux partitioning. Biogeosciences 9 (12), 5243–5259.
897 URL http://www.biogeosciences.net/9/5243/2012/

Lavigne, M., Franklin, S., Hunt, E.R., J., 1996. Estimating stem maintenance respiration rates of dissimilar balsam fir stands. Tree Physiology 16, 687–695.
URL https://www.researchgate.net/profile/Michael_Lavigne2/publication/8778227_Estimating_stem_maintenance_respiration_rates_of_dissimilar_balsam_fir_stands/links/02e7e51819154d8e72000000.pdf

Li, L., Njoku, E. G., Im, E., Chang, P. S., Germain, K. S., 2004. A preliminary survey of radio-frequency interference over the u.s. in aqua AMSR-e data 42 (2), 380–390.

Liu, P.-W., Judge, J., DeRoo, R. D., England, A. W., Bongiovanni, T., Luke, A., 2016. Dominant backscattering mechanisms at L-band during dynamic soil moisture conditions for sandy soils. Remote Sensing of Environment 178, 104–112.
URL http://www.sciencedirect.com/science/article/pii/S0034425716300918

Liu, Y. Y., Evans, J. P., McCabe, M. F., de Jeu, R. A. M., van Dijk, A. I. J. M., Dolman, A. J., Saizen, I., 2013a. Changing Climate and Overgrazing Are Decimating Mongolian Steppes. PLoS ONE 8 (2), e57599.
URL http://dx.plos.org/10.1371/journal.pone.0057599

Liu, Y. Y., Jeu, D., M, R. A., McCabe, M. F., Evans, J. P., Dijk, V., M, A. I. J., 2011. Global long-term passive microwave satellite-based retrievals of

vegetation optical depth. Geophysical Research Letters 38 (18).
URL http://onlinelibrary.wiley.com/doi/10.1029/2011GL048684/abstract

Liu, Y. Y., van Dijk, A. I. J. M., de Jeu, R. A. M., Canadell, J. G., McCabe, M. F., Evans, J. P., Wang, G., 2015. Recent reversal in loss of global terrestrial biomass. Nature Climate Change 5 (5), 470–474.
URL http://www.nature.com/doifinder/10.1038/nclimate2581

Liu, Y. Y., van Dijk, A. I. J. M., de Jeu, R. A. M., Holmes, T. R. H., 2009. An analysis of spatiotemporal variations of soil and vegetation moisture from a 29-year satellite-derived data set over mainland Australia. Water Resources Research 45 (7), W07405.
URL http://onlinelibrary.wiley.com/doi/10.1029/2008WR007187/abstract

Liu, Y. Y., van Dijk, A. I. J. M., McCabe, M. F., Evans, J. P., de Jeu, R. A. M., 2013b. Global vegetation biomass change (1988-2008) and attribution to environmental and human drivers: Global vegetation biomass change. Global Ecology and Biogeography 22 (6), 692–705.
URL http://doi.wiley.com/10.1111/geb.12024

Marle, M. J. E. v., Werf, G. R. v. d., Jeu, R. A. M. d., Liu, Y. Y., 2016. Annual South American forest loss estimates based on passive microwave remote sensing (1990-2010). Biogeosciences 13 (2), 609–624.

URL http://www.biogeosciences.net/13/609/2016/bg-13-609-2016-relations.html

Martens, B., Miralles, D. G., Lievens, H., van der Schalie, R., de Jeu, R. A. M., Férnandez-Prieto, D., Beck, H. E., Dorigo, W. A., Verhoest, N. E. C., 2016. GLEAM v3: satellite-based land evaporation and root-zone soil moisture. Geoscientific Model Development Discussions, 1–36.
URL http://www.geosci-model-dev-discuss.net/gmd-2016-162/

Meesters, A. G. C. A., Jeu, R. A. M. D., Owe, M., 2005. Analytical derivation of the vegetation optical depth from the microwave polarization difference index. IEEE Geoscience and Remote Sensing Letters 2 (2), 121–123.
URL http://ieeexplore.ieee.org/articleDetails.jsp?arnumber=1420287

Melzer, T., 2013. Vegetation Modelling in WARP 6.0. In: Understanding the past, observing the present and protecting the future Vienna 2013. Vienna, Austria.

Miralles, D. G., Holmes, T. R. H., De Jeu, R. A. M., Gash, J. H., Meesters, A. G. C. A., Dolman, A. J., 2011. Global land-surface evaporation estimated from satellite-based observations. Hydrology and Earth System Sciences 15 (2), 453–469.
URL http://search.proquest.com/openview/

962 e97bc7142dade93942375ef83bde1590/1?pq-origsite=gscholar&
963 cbl=105724

964 Miralles, D. G., Nieto, R., McDowell, N. G., Dorigo, W. A., Verhoest, N. E.,
965 Liu, Y. Y., Teuling, A. J., Dolman, A. J., Good, S. P., Gimeno, L., 2016.
966 Contribution of water-limited ecoregions to their own supply of rainfall.
967 Environmental Research Letters 11 (12), 124007.
968 URL http://iopscience.iop.org/article/10.1088/1748-9326/11/
969 12/124007/meta

970 Mo, T., Choudhury, B. J., Schmugge, T. J., Wang, J. R., Jackson, T. J.,
971 1982. A model for microwave emission from vegetation-covered fields.
972 Journal of Geophysical Research: Oceans 87 (C13), 11229–11237.
973 URL http://onlinelibrary.wiley.com/doi/10.1029/
974 JC087iC13p11229/full

975 Monteith, J. L., 1972. Solar Radiation and Productivity in Tropical Ecosys-
976 tems. Journal of Applied Ecology 9 (3), 747–766.
977 URL http://www.jstor.org/stable/2401901

978 Morton, D. C., Nagol, J., Carabajal, C. C., Rosette, J., Palace, M., Cook,
979 B. D., Vermote, E. F., Harding, D. J., North, P. R. J., 2014. Amazon
980 forests maintain consistent canopy structure and greenness during the dry
981 season. Nature 506 (7487), 221–224.
982 URL http://www.nature.com/doifinder/10.1038/nature13006

983 Myneni, R. B., Hoffman, S., Knyazikhin, Y., Privette, J. L., Glassy, J., Tian,
984 Y., Wang, Y., Song, X., Zhang, Y., Smith, G. R., Lotsch, A., Friedl, M.,
985 Morisette, J. T., Votava, P., Nemani, R. R., Running, S. W., 2002. Global
986 products of vegetation leaf area and fraction absorbed PAR from year one
987 of MODIS data. Remote Sensing of Environment 83 (1–2), 214–231.
988 URL http://www.sciencedirect.com/science/article/pii/
989 S0034425702000743

990 Nemani, R. R., Keeling, C. D., Hashimoto, H., Jolly, W. M., Piper, S. C.,
991 Tucker, C. J., Myneni, R. B., Running, S. W., 2003. Climate-Driven In-
992 creases in Global Terrestrial Net Primary Production from 1982 to 1999.
993 Science 300 (5625), 1560–1563.
994 URL http://science.sciencemag.org/content/300/5625/1560

995 Njoku, E. G., Ashcroft, P., Chan, T. K., Li, L., 2005. Global survey and
996 statistics of radio-frequency interference in AMSR-e land observations
997 43 (5), 938–947.

998 Nunes, L., Lopes, D., Castro Rego, F., Gower, S. T., 2013. Aboveground
999 biomass and net primary production of pine, oak and mixed pine–oak
1000 forests on the Vila Real district, Portugal. Forest Ecology and Manage-
1001 ment 305, 38–47.
1002 URL https://www.sciencedirect.com/science/article/pii/
1003 S0378112713003332

1004 Olivares, E., Medina, E., 1992. Water and nutrient relations of woody peren-

nials from tropical dry forests. Journal of Vegetation Science 3 (3), 383–392.
URL http://onlinelibrary.wiley.com/doi/10.2307/3235764/full

Owe, M., de Jeu, R., Holmes, T., 2008. Multisensor historical climatology of satellite-derived global land surface moisture 113, F01002.
URL http://onlinelibrary.wiley.com/doi/10.1029/2007JF000769/abstract

Owe, M., Jeu, R. d., Walker, J., 2001. A methodology for surface soil moisture and vegetation optical depth retrieval using the microwave polarization difference index. IEEE Transactions on Geoscience and Remote Sensing 39 (8), 1643–1654.
URL http://ieeexplore.ieee.org/articleDetails.jsp?arnumber=942542

Papagiannopoulou, C., Miralles, D. G., Dorigo, W. A., Verhoest, N. E. C., Depoorter, M., Waegeman, W., 2017. Vegetation anomalies caused by antecedent precipitation in most of the world 12 (7), 074016.
URL http://stacks.iop.org/1748-9326/12/i=7/a=074016?key=crossref.aec129902b307d6614b07d44903e2fe7

Reichstein, M., Falge, E., Baldocchi, D., Papale, D., Aubinet, M., Berbigier, P., Bernhofer, C., Buchmann, N., Gilmanov, T., Granier, A., Grünwald, T., Havránková, K., Ilvesniemi, H., Janous, D., Knohl, A., Laurila, T., Lohila, A., Loustau, D., Matteucci, G., Meyers, T., Miglietta, F.,

1026 Ourcival, J.-M., Pumpanen, J., Rambal, S., Rotenberg, E., Sanz, M.,
1027 Tenhunen, J., Seufert, G., Vaccari, F., Vesala, T., Yakir, D., Valentini, R.,
1028 2005. On the separation of net ecosystem exchange into assimilation and
1029 ecosystem respiration: review and improved algorithm 11 (9), 1424–1439.
1030 URL http://onlinelibrary.wiley.com/doi/10.1111/j.1365-2486.
1031 2005.001002.x/abstract

1032 Rogers, A., Medlyn, B. E., Dukes, J. S., Bonan, G., von Caemmerer, S.,
1033 Dietze, M. C., Kattge, J., Leakey, A. D. B., Mercado, L. M., Niinemets,
1034 l., Prentice, I. C., Serbin, S. P., Sitch, S., Way, D. A., Zaehle, S., 2017.
1035 A roadmap for improving the representation of photosynthesis in earth
1036 system models 213 (1), 22–42.
1037 URL http://onlinelibrary.wiley.com/doi/10.1111/nph.14283/
1038 abstract

1039 Running, S. W., Nemani, R. R., Heinsch, F. A., Zhao, M., Reeves, M.,
1040 Hashimoto, H., 2004. A Continuous Satellite-Derived Measure of Global
1041 Terrestrial Primary Production. BioScience 54 (6), 547–560.
1042 URL http://bioscience.oxfordjournals.org/content/54/6/547

1043 Ryan, M. G., 1990. Growth and maintenance respiration in stems of Pi-
1044 nuscontorta and Piceaengelmannii. Canadian Journal of Forest Research
1045 20 (1), 48–57.
1046 URL http://www.nrcresearchpress.com/doi/abs/10.1139/x90-008#
1047 .WPf7HGclHmg

Sawada, Y., Tsutsui, H., Koike, T., Rasmy, M., Seto, R., Fujii, H., 2016. A Field Verification of an Algorithm for Retrieving Vegetation Water Content From Passive Microwave Observations. IEEE Transactions on Geoscience and Remote Sensing 54 (4), 2082–2095.

Scurlock, J. M. O., Johnson, K., Olson, R. J., 2002. Estimating net primary productivity from grassland biomass dynamics measurements. Global Change Biology 8 (8), 736–753.
URL http://onlinelibrary.wiley.com/doi/10.1046/j.1365-2486.2002.00512.x/full

Suyker, A. E., Verma, S. B., Burba, G. G., Arkebauer, T. J., 2005. Gross primary production and ecosystem respiration of irrigated maize and irrigated soybean during a growing season. Agricultural and Forest Meteorology 131 (3–4), 180–190.
URL http://www.sciencedirect.com/science/article/pii/S0168192305001127

Tian, F., Brandt, M., Liu, Y. Y., Verger, A., Tagesson, T., Diouf, A. A., Rasmussen, K., Mbow, C., Wang, Y., Fensholt, R., 2016. Remote sensing of vegetation dynamics in drylands: Evaluating vegetation optical depth (VOD) using AVHRR NDVI and in situ green biomass data over West African Sahel. Remote Sensing of Environment 177, 265–276.
URL http://linkinghub.elsevier.com/retrieve/pii/S0034425716300852

Tramontana, G., Jung, M., Schwalm, C. R., Ichii, K., Camps-Valls, G., Ráduly, B., Reichstein, M., Arain, M. A., Cescatti, A., Kiely, G., Merbold, L., Serrano-Ortiz, P., Sickert, S., Wolf, S., Papale, D., 2016. Predicting carbon dioxide and energy fluxes across global FLUXNET sites with regression algorithms. Biogeosciences 13 (14), 4291–4313.
URL http://www.biogeosciences.net/13/4291/2016/bg-13-4291-2016-metrics.html

USGS, 1996. Global 30-Arc-Second Elevation Data Set (GTOPO30).
URL http://lpdaac.usgs.gov

van der Schalie, R., de Jeu, R. A. M., Kerr, Y. H., Wigneron, J. P., Rodríguez-Fernández, N. J., Al-Yaari, A., Parinussa, R. M., Mecklenburg, S., Drusch, M., 2017. The merging of radiative transfer based surface soil moisture data from SMOS and AMSR-E. Remote Sensing of Environment 189, 180–193.
URL http://www.sciencedirect.com/science/article/pii/S0034425716304734

van der Schalie, R., Kerr, Y. H., Wigneron, J. P., Rodríguez-Fernández, N. J., Al-Yaari, A., Jeu, R. A. M. d., 2016. Global SMOS Soil Moisture Retrievals from The Land Parameter Retrieval Model. International Journal of Applied Earth Observation and Geoinformation 45, Part B, 125–134.

URL http://www.sciencedirect.com/science/article/pii/S0303243415300179

Verbesselt, J., Umlauf, N., Hirota, M., Holmgren, M., Van Nes, E. H., Herold, M., Zeileis, A., Scheffer, M., 2016. Remotely sensed resilience of tropical forests. Nature Climate Change 6 (11), 1028–1031.
URL http://www.nature.com/doifinder/10.1038/nclimate3108

Vreugdenhil, M., Dorigo, W. A., Wagner, W., Jeu, R. A. M. d., Hahn, S., Marle, M. J. E. v., 2016a. Analyzing the Vegetation Parameterization in the TU-Wien ASCAT Soil Moisture Retrieval. IEEE Transactions on Geoscience and Remote Sensing 54 (6), 3513–3531.
URL http://ieeexplore.ieee.org/articleDetails.jsp?arnumber=7410033

Vreugdenhil, M., Hahn, S., Melzer, T., Bauer-Marschallinger, B., Reimer, C., Dorigo, W. A., Wagner, W., 2016b. Assessing Vegetation Dynamics Over Mainland Australia With Metop ASCAT. IEEE Journal of Selected Topics in Applied Earth Observations and Remote Sensing PP (99), 1–9.

Wagner, F., Rossi, V., Stahl, C., Bonal, D., Hérault, B., 2013a. Asynchronism in leaf and wood production in tropical forests: a study combining satellite and ground-based measurements. Biogeosciences 10 (11), 7307–7321.
URL http://www.biogeosciences.net/10/7307/2013/

Wagner, W., Hahn, S., Kidd, R., Melzer, T., Bartalis, Z., Hasenauer, S.,

Figa-Saldaña, J., de Rosnay, P., Jann, A., Schneider, S., Komma, J., Kubu, G., Brugger, K., Aubrecht, C., Züger, J., Gangkofner, U., Kienberger, S., Brocca, L., Wang, Y., Blöschl, G., Eitzinger, J., Steinnocher, K., Zeil, P., Rubel, F., 2013b. The ASCAT Soil Moisture Product: A Review of its Specifications, Validation Results, and Emerging Applications. Meteorologische Zeitschrift 22 (1), 5–33.

Waring, R. H., Landsberg, J. J., Williams, M., 1998. Net primary production of forests: a constant fraction of gross primary production? Tree Physiology 18 (2), 129–134.
URL http://treephys.oxfordjournals.org/content/18/2/129

Woodhouse, I. H., 2005. Introduction to Microwave Remote Sensing. CRC Press.

Wright, S. J., van Schaik, C. P., 1994. Light and the Phenology of Tropical Trees. American Naturalist 143 (1), 192–199.
URL http://www.jstor.org/stable/2462858?seq=1#page_scan_tab_contents

Zhang, Y., Guanter, L., Berry, J. A., Tol, C. v. d., Joiner, J., 2016. Can we retrieve vegetation photosynthetic capacity paramter from solar-induced fluorescence? In: 2016 IEEE International Geoscience and Remote Sensing Symposium (IGARSS). pp. 1711–1713.

Zhao, M., Heinsch, F. A., Nemani, R. R., Running, S. W., 2005. Improve-

ments of the MODIS terrestrial gross and net primary production global data set. Remote Sensing of Environment 95 (2), 164–176.
URL http://www.sciencedirect.com/science/article/pii/S0034425705000106

Zribi, M., Chahbi, A., Shabou, M., Lili-Chabaane, Z., Duchemin, B., Baghdadi, N., Amri, R., Chehbouni, A., 2011. Soil surface moisture estimation over a semi-arid region using ENVISAT ASAR radar data for soil evaporation evaluation. Hydrology and Earth System Sciences Discussions 15 (1), 345–358.
URL http://hal.ird.fr/ird-00610514/document